AN EMPIRICALLY DERIVED LUNAR GRAVITY FIELD

A. J. FERRARI
Bellcomm, Inc., Washington, D.C., U.S.A.

(Received 13 January, 1972)

Abstract. A new method has been devised to determine spherical harmonic coefficients of the lunar gravity field. This method uses a two-step data reduction and estimation process. The first step applies a weighted least-squares empirical orbit determination process to Doppler tracking data to estimate long-period Kepler elements and rates. In the second step, lunar gravity coefficients are determined using another weighted least-squares processor which fits the long-period Lagrange perturbation equations to the estimated Keplerian rates.

This method has been applied to tracking data from the Lunar Orbiter missions. A gravity potential of degree and order four is presented and error sources discussed. Plots of lunar equipotential surfaces are shown. Gravity field results are applied to various physical properties of the Moon such as moments and products of inertia. This gravity field has been investigated using data from several Apollo missions. Solutions from these data, in all cases except that of Apollo 15, result in improved orbit predictions as compared to those using other fields. All solutions indicate that the field models are still imcomplete.

1. Introduction

A new method for determining the spherical harmonic coefficients of the lunar gravitational potential is applied to Doppler tracking data from the Lunar Orbiter satellites. This selenodesy scheme consists of two separate data reduction and estimation processes. First Doppler data are reduced and estimates obtained for the long-period Kepler elements and element rates of the orbit. These rates are used as input to a second processor which utlizes the long-period Lagrange perturbation equations to determine a finite set of lunar gravity coefficients.

This paper presents a lunar gravity model obtained using this method. Analyses are also included which illustrate some of the characteristic properties of the model.

2. Mathematical Theory*

The dynamical state ($\mathbf{k}$) of a satellite in lunar orbit, referenced to Moon-centered inertial coordinates, is defined by the six-vector of long-period Kepler elements (a, e, I, ω, Ω, M) (see Figure 1). The equations of motion are the six first-order, non-linear, long-period Lagrange perturbation equations [1]

$$\frac{d\mathbf{k}}{dt} = \mathbf{f}(\mathbf{k}', \mathbf{p}, t), \tag{1}$$

where $\mathbf{k}'$ is the vector of Kepler elements excluding the mean anomaly and $\mathbf{p}$ is the vector of spherical harmonics of lunar gravity. The function $\mathbf{f}(\mathbf{k}', \mathbf{p}, \mathbf{t})$ appearing in

* Reference [5] gives more details of this method and presents a successful pseudo data test.

The Moon **5** (1972) 390–410.

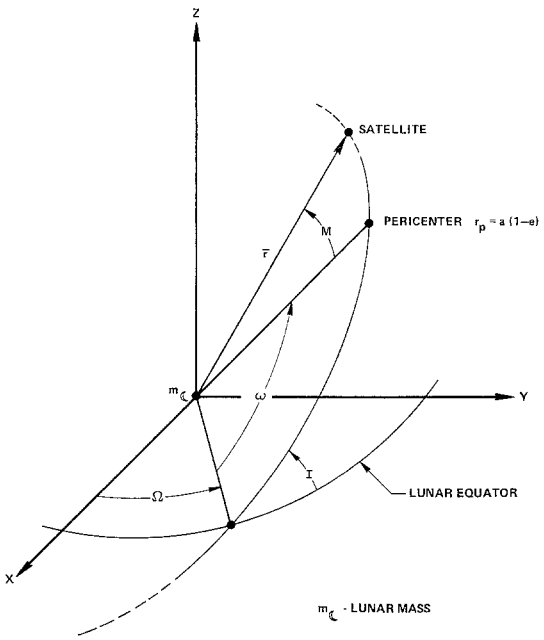

Fig. 1. Geometry of orbital elements.

Equation (1) is assumed to be composed of the sum of perturbations arising from non-central lunar gravity [2], Earth and Sun gravity [3], and solar radiation pressure [4].

The vector of spherical harmonic coefficients appearing in Equation (1) is related to the lunar gravitational potential as prescribed by the solution to the Laplace equation ($\nabla^2 U = 0$) expressed in Moon-fixed spherical coordinates

$$U = \frac{\mu_{\mathbb{C}}}{r}\left[1 + \sum_{l=2}^{\infty}\sum_{m=0}^{l}\left(\frac{R_e}{r}\right)^l P_l^m(\sin\phi)\{C_{lm}\cos m\lambda + S_{lm}\sin m\lambda\}\right]. \tag{2}$$

In this equation R_e is the mean radius of the Moon, P_l^m is the associated Legendre polynomial, (r, ϕ, λ) are the selenographic radius, latitude, and longitude, $\mu_{\mathbb{C}}$ is the lunar gravity constant, and $\{C_{lm}, S_{lm}\}$ are the spherical harmonic coefficients (components of **p**) which describe the non-central features of the Moon. The terms of the first degree ($l=1$) are omitted from the series expansion since it is assumed that the origin of coordinates and the center of mass of the Moon are coincident.

A solution to Equation (1), valid for a period of up to a day, can be accurately approximated by the following six-dimensional time series [5]

$$\mathbf{k}(t) = \mathbf{K}_0 + \mathbf{K}_1 t + \mathbf{K}_2 t^2 + \delta\mathbf{k}_{\oplus} + \delta\mathbf{k}_{\odot} + \delta\mathbf{k}_{sr}. \tag{3}$$

The terms $\mathbf{K}_0$, $\mathbf{K}_1$, $\mathbf{K}_2$ are Keplerian constants determined in the first processor by least-squares fitting of Doppler tracking data. The orbital element variations $\delta\mathbf{k}_{\oplus}$,

$\delta\mathbf{k}_{\odot}$, and $\delta\mathbf{k}_{sr}$ are those arising from Earth, Sun, and solar radiation pressure perturbations. Explicit representations are used for third body and solar pressure effects and the variations are obtained by numerical integration. The Keplerian parameters estimated by this step of the method are ascribed to the non-central features of the Moon.

The weighted least-squares process for obtaining the Keplerian parameters is formulated as

$$\Delta\tilde{K} = [H^T W H]^{-1} H^T W \Delta\dot{\varrho}, \tag{4}$$

where $\Delta\tilde{K}$ is the column vector of Keplerian parameters, H is a linearized set of functions relating the Doppler to the Keplerian parameters, W is a diagonal weighting matrix (the reciprocal of the Doppler variance), and $\Delta\dot{\varrho}$ is the column vector of Doppler residuals. Since Equation (4) represents a linearization of a non-linear set of equations, it is solved iteratively.

Analyses [6] have shown that the least-squares process has convergence problems when the semi-major axis is included as an independent parameter. In order to alleviate this situation, the estimated mean motion is used to imply a semi-major axis. The constraint equation used must include a representation for the lunar field. The L1 gravity model [7] was used in this analysis. The average value of the semi-major axis (a_0) with respect to the mean anomaly is found from

$$\hat{\dot{M}} = \hat{\dot{M}}_1 + 2\hat{\dot{M}}_2 t + \dot{M}_{\oplus} + \dot{M}_{\odot} + \dot{M}_{sr} \tag{5}$$

and

$$\hat{\dot{M}} = \sqrt{\frac{\mu_{\mathbb{C}}}{a_0^3}} + \dot{M}_{\mathrm{L1}}(a_0),$$

where $\hat{\dot{M}}_1$ and $\hat{\dot{M}}_2$ are the estimated Keplerian parameters. Since this is a non-linear equation in a_0, it is solved using an iterative method.

Kozai [8] has shown that the average satellite radial distance in the orbit is obtained only when a mean value ($\bar{a}$) of the semi-major axis is used. This value is derived such that the deviations between the osculating and the long-period radius due to perturbations averaged over the orbit yield only short-period variations. Hence the value $\bar{a}$ yields the proper mean radius in the orbit. A mean value correction is only required for the C_{20} zonal term [9] and the Earth effect. Analysis has shown that mean value corrections for the Sun and solar radiation pressure are negligible. The mean value $\bar{a}$ is calculated from

$$\bar{a} = a_0[1 + \varepsilon_{20} + \varepsilon_{\oplus}], \tag{6}$$

where the ε terms are the mean value corrections. Since the quantity $\bar{a}$ is only introduced to insure compatibility between the long-period and associated rectangular equations of motion, it is only used for Doppler data reduction.

The output from processing a batch of Doppler measurements is a best estimate for a set of Keplerian parameters, $\tilde{K}$. These solution parameters give a simultaneous

time history of the Kepler elements and element rates valid over the Doppler tracking span. A detailed block diagram of the orbit determination process is shown in Figure 2. Since the solution parameters provide continuous time functions of the orbital elements and rates they can be sampled at any desired time. Long-period lunar gravity effects have periods which are much greater than a typical lunar orbiter period, hence there will be no aliasing of gravity information if samples are evaluated once per satellite period.

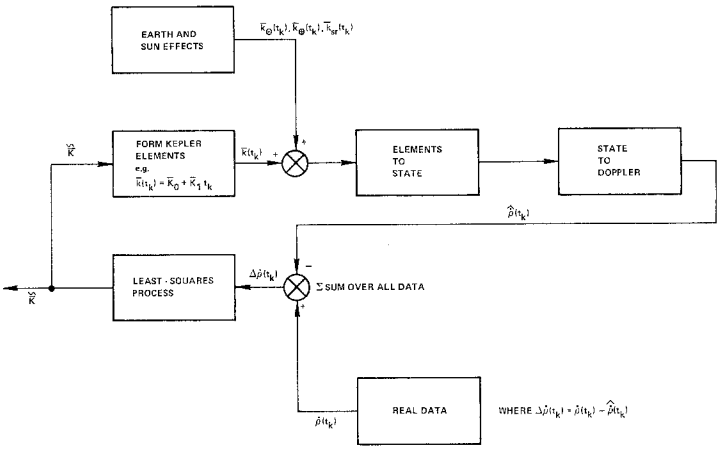

Fig. 2. Orbit determination block diagram.

The five orbital element rates are simultaneously processed in a second least-squares estimator to obtain lunar gravity coefficients. Since the data set consists of five different quantities, a weighting matrix is required to define the relative accuracy of each of the rates.

Only long-period satellite dynamics are represented in the first processor, hence the $[H^T W H]^{-1}$ matrix is not the covariance matrix of the estimates. [10] However, since the terms in the $[H^T W H]^{-1}$ matrix do reflect the sensitivity and correlations among the solution parameters, it is assumed for weighting purposes that these terms can be used in the conventional manner. [11] The weighting matrix, A, for the orbital elements is of the form

$$A^{-1} = \begin{bmatrix} \sigma^2_{\hat{e}} & \tau_{12} & \tau_{13} & \tau_{14} & \tau_{15} \\ \tau_{21} & \sigma^2_{\hat{i}} & \cdots & \cdots & \cdots \\ \vdots & & \sigma^2_{\hat{\Omega}} & \cdots & \cdots \\ \text{Symmetric} & & & \sigma^2_{\hat{\omega}} & \cdots \\ \tau_{51} & \cdots & \cdots & \cdots & \sigma^2_{\hat{M}} \end{bmatrix}, \tag{7}$$

where $\sigma^2_{\hat{k}}$ are the error variances among the rates and τ_{ij} are the error covariances.

The lunar gravity field determination is performed in a second weighted least-squares processor which uses as input the Kepler element rates, the Kepler elements

and a weighting matrix (see Figure 3). The long-period perturbation equations for the non-central lunar gravity only are

$$\dot{\mathbf{k}} = \mathbf{g}(\mathbf{k}', \mathbf{p}, t). \tag{8}$$

Since the gravity parameters appear as linear functions in the perturbation equations, Equation (8) can be expressed as

$$\dot{\mathbf{k}} = G(\mathbf{k}')\,\mathbf{p}, \tag{9}$$

where G is a matrix of partial derivatives of the element rates with respect to the gravity coefficients. The least-squares algorithm for gravity coefficient estimation is of the form

$$\hat{\mathbf{p}} = [G^T A G]^{-1} G^T A \dot{\mathbf{k}}, \tag{10}$$

where $\hat{\mathbf{p}}$ is the best estimate of lunar gravity parameters.

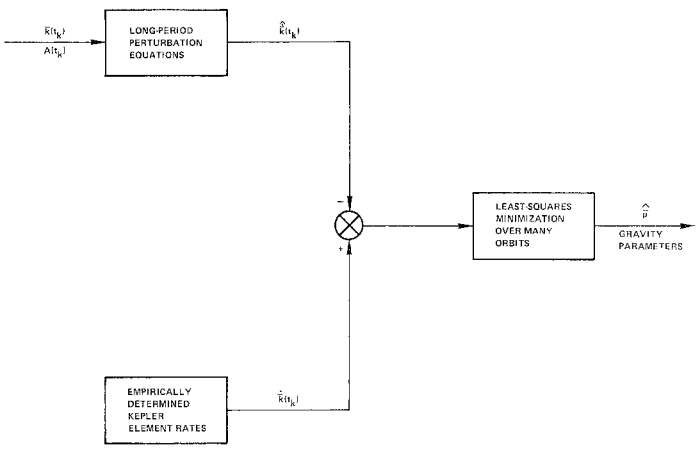

Fig. 3. Gravity coefficient estimation.

3. Data Analysis

Large amounts of Doppler tracking data were acquired during the lunar orbits of both the Lunar Orbiter (1–5) and the Apollo (8, 10, 11, 12, 14, and 15) missions. Almost all the tracking data acquired during the photographic portions of the Lunar Orbiter missions include propulsive attitude control maneuvers performed at such a high frequency (about every three hours) that these data cannot be used for selenodesy purposes. Even the Lunar Orbiter data from the extended mission phases (primarily that used in this analysis) contains some minor propulsive thrusts. Data from all the Apollo 8 mission and large portions of the Apollo 10, 11, and 15 missions contain propulsive thrusting. The extended mission phase Lunar Orbiter data were used to determine the lunar gravity field presented in this study since it is not only

the largest but also the most complete data set gathered to date.* The free-flight quality data from parts of the Apollo 11, 12, and 14 missions were used as control data to test the quality of the lunar field obtained. The small amount of Apollo data which is of free-flight quality cannot be used in the method since these data are from nearly circular and nearly equatorial orbits and the method as it has been developed becomes singular for orbits of this type.

The epoch times, length, and number of tracking stations of the various data arcs used in this analysis are listed in Table I. No data from the Lunar Orbiter 4 satellite were included; since earth perturbations were very dominant for this orbit. It was assumed to have only minimal spherical harmonic content. The length of the data arcs used in orbit determination solutions varies from a minimum of about eight hours to a maximum of thirty six hours.

TABLE I

Lunar orbiter data arcs

Satellite	Epoch (Day, Mo., Yr.)			Length (s)	Stations
Orbiter 1	31.41180556	Aug.	1966	75989	3
	1.32430556	Sept.	1966	88889	3
	4.22916667	Sept.	1966	84000	3
	13.84722222	Sept.	1966	81000	3
	14.81597222	Sept.	1966	81000	3
	15.78263889	Sept.	1966	108670	3
Orbiter 2	8.85938421	Dec.	1966	92700	3
	10.55208333	Dec.	1966	32760	3
	29.61805556	June	1967	34260	2
Orbiter 3	20.60000000	Feb.	1967	93290	3
	21.68055556	Feb.	1967	86000	3
	27.97222222	Feb.	1967	89280	3
	2.38194444	Mar.	1967	75000	3
	5.16666667	Mar.	1967	110800	3
	6.83958333	Mar.	1967	97740	3
	24.21527778	Mar.	1967	31380	2
	11.48611111	April	1967	46080	2
Orbiter 5	18.31111111	Aug.	1967	63000	3
	19.09027778	Aug.	1967	88000	3
	20.11111111	Aug.	1967	119450	3
	21.49652778	Aug.	1967	119068	3
	24.21180556	Aug.	1967	87928	3
	25.22847222	Aug.	1967	59340	3
	26.25208333	Aug.	1967	85000	3
	27.28819444	Aug.	1967	70468	3
	2.52777778	Oct.	1967	29880	2
	3.54166667	Oct.	1967	43200	2
	17.38194444	Nov.	1967	38040	2
	21.31944444	Nov.	1967	33568	2
	29.86111111	Jan.	1968	112618	3

* These data are far from complete in an absolute sense since the Lunar Orbiter Satellites were in either very high ($I=85°$) or relatively low ($I=21°$) inclined orbits.

Two different sized parameter sets were used to represent the Keplerian satellite state in lunar orbit. The first set contains eleven parameters $\{e_0, e_1, I_0, I_1, \Omega_0, \Omega_1 \omega_0, \omega_1, M_0, M_1, M_2\}$ and was used exclusively when the Doppler data span was twelve hours or less. The second solution set contains thirteen parameters $\{e_0, e_1, e_2, I_0, I_1, \Omega_0, \Omega_1, \Omega_2, \omega_0, \omega_1, \omega_2, M_0, M_1, M_2\}$ and was used when the data span was greater than twelve hours. Analysis with pseudo data showed that this choice of parameters should be adequate to model the long-period variations of the satellite.

Table II contains all the astrodynamical constants assumed known and fixed in the orbit determination processor and a list of the tracking station locations. The positions and relative velocities of the Earth, Sun, and Moon were obtained from Jet Propulsion Laboratory Ephemeris Tape DE-19. [12]

The rate of convergence for each orbit determination solution varied as a function of the orbit, the data arc length, and the number and location of the Earth based stations used. In general each convergence took about five to six iterations. The numerical particulars associated with a typical solution for each of the Lunar Orbiters (1, 2, 3, and 5) are now discussed.

TABLE II

Physical constants

I. *Astrodynamic constants*

Gravitational parameters:

$\mu_{\leftmoon} = 0.173\,130\,041\,708\,779\,8 \times 10^{15}$ ft^3 s^{-2}

$\mu_{\oplus} = 0.140\,764\,685\,327\,854\,2 \times 10^{17}$ ft^3 s^{-2}

$\mu_{\odot} = 0.468\,669\,767\,196\,088\,8 \times 10^{22}$ ft$^{3\ -2}$

Mean lunar radius:

$R_e = 0.570\,239\,501\,312\,336 \times 10^7$ ft

Angular velocity of Moon's rotation:

$\gamma = 0.266\,170\,331\,689\,165\,7 \times 10^{-5}$ rad s^{-1}

Velocity of light in a vacuum:

$c = 0.983\,571\,194\,225\,721\,8 \times 10^9$ ft s^{-1}

II. *Station locations*

Station	Geocentric coordinates		
	radius, ft.	latitude, deg.	longitude, deg.
Goldstone, Calf. (DSS12)	20905479	35.118640	243.19483
Woomera, Australia (DSS41)	20907326	-31.211390	136.88779
Madrid, Spain (DSS61)	20898911	40.238540	355.75129
Madrid, Spain (DSS62)	20898927	40.263490	355.63246

III. *Doppler data weight* $W = \frac{1}{\sigma^2}$, $\sigma = 0.00213$ ft s^{-1}

IV. *Solar acceleration* $F = 3.973 \times 10^{-7}$ ft s^{-2}

Representative residuals from Lunar Orbiter 1, 2, 3, and 5 orbit determination solutions are shown in Figures 4 and 5. The residuals associated with each of these convergences have the statistical properties listed in Table III. As can be seen from the figures, the residuals associated with the Lunar Orbiter 1 and 2 convergences presented have larger peak amplitudes. Each of these plots also possesses points of irregularly large amplitude relative to the remainder of the span. These irregularities in the residuals most likely correspond to low thrust attitude control maneuvers performed by the spacecraft.

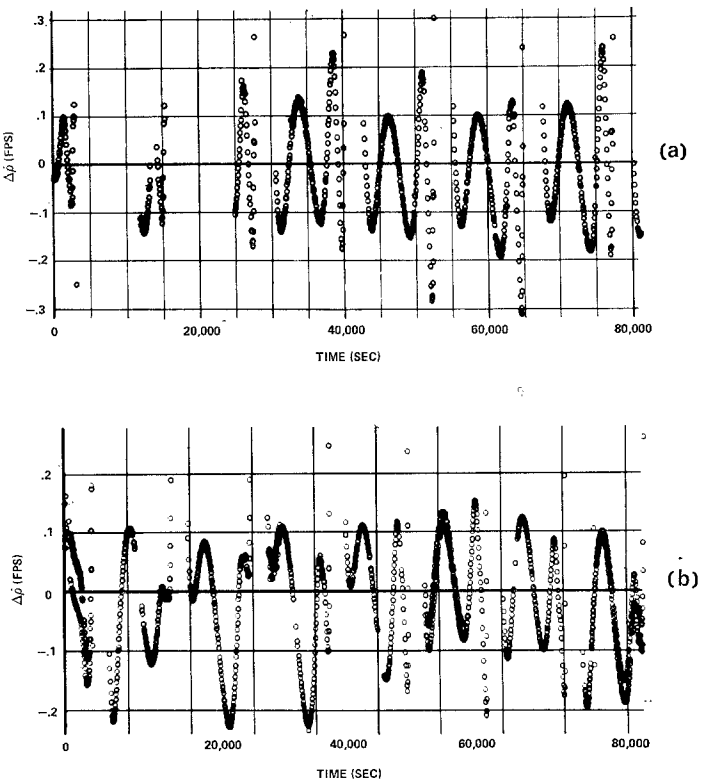

Fig. 4. (a) Lunar Orbiter 1 and (b) Lunar Orbiter 2 Doppler residuals vs. time.

TABLE III

Lunar Orbiter Doppler residual statistics

Satellite	Residual mean (fps)	Residual std. deviation (fps)
Orbiter 1	−0.010	0.108
Orbiter 2	−0.012	0.090
Orbiter 3	0.006	0.053
Orbiter 5	0.003	0.068

An analysis of the $[H^T WH]^{-1}$ matrix for each of these solutions shows that many of the Keplerian parameters are extremely highly correlated. Table IV presents a summary of the highest correlations for each of these four convergences. These correlations are the largest found in each $[H^T WH]^{-1}$ matrix. Other correlations were

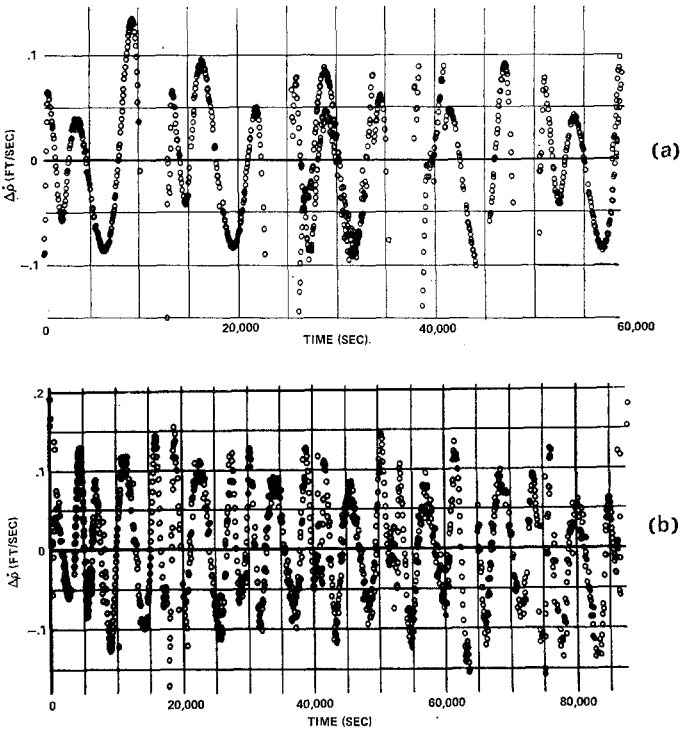

Fig. 5. (a) Lunar Orbiter 3 and (b) Lunar Orbiter 5 Doppler residuals.

TABLE IV
Solution correlations

Satellite	Parameter pair	Correlation coef.
Orbiter 1	Ω_0, ω_0	−0.9999
	Ω_1, ω_1	0.9999
Orbiter 2	I_0, Ω_0	−0.9908
	Ω_0, ω_0	−0.9998
	Ω_1, ω_1	−0.9995
Orbiter 3	I_0, Ω_0	−0.9938
	I_0, ω_0	−0.9946
	Ω_0, ω_0	−0.9998
	Ω_1, ω_1	−0.9985
Orbiter 5	I_0, Ω_0	0.9948
	I_0, ω_0	−0.9903
	Ω_0, ω_0	−0.9843
	$\Omega_1, I_1,$	0.9948

also present of large magnitude ($|\varrho| \geqslant 0.9$). For the case of each Lunar Orbiter satellite presented almost the identical correlation pairs reoccur. These correlations reflect the basic difficulty of using Doppler measurements at lunar distances to separate the dynamical properties of the Euler angles of the orbit. It should be noted that this situation is particularly amplified for the case of the Lunar Orbiters since in most cases the satellite was only tracked by one earth based station, thus losing the geometrical enhancement of a second or third tracker.

The thirty data arcs used for orbit determination solutions contributed one hundred ninety-nine sets of Kepler elements and element rates for lunar gravity determination. The factors used in defining the degree and order of the lunar field determined from these sets of Kepler elements and rates are now discussed.

4. A Priori Coefficient Selection

The work of Muller and Sjogren [13] has provided conclusive evidence that rather large near-surface mass concentrations (mascons) are present in the near-side lunar maria regions. The existence of these non-central mass concentrations has significant impact on the application of Equation (2) for describing lunar gravity. Accurately representing a mascon moon would require spherical harmonic coefficients of high degree and order. In mathematical teminology, the presence of a mascon causes the convergence rate of Equation (2) to be very slow.

In theory the proper approach to modeling the lunar gravity field is to seek a spherical harmonic coefficient set large enough in degree and order to represent all the non-central lunar features. In practice, however, due to the incomplete Doppler data set and due to a lack of far side Doppler measurements, lunar gravity solutions involving large numbers of harmonic coefficients have high correlations in the $[G^TAG]^{-1}$ matrix and in general have poor overall numerical characteristics.

Analyses were made using the harmonic estimating processor with pseudo data input from numerically integrated long-period perturbation equations (assuming a nominal seventh degree and order lunar field). Long-period trajectories for each of the Lunar Orbiter missions were simulated. When a solution set of degree and order seven or larger was sought, the nominal values of the field were recovered with excellent accuracy. An analysis of the correlations in the $[G^TAG]^{-1}$ matrices for these solutions showed that a great many harmonic coefficient pairs (C_{20} and C_{40}, C_{30} and C_{50}, etc.) were very highly correlated. This correlation is totally a consequence of the incomplete data set used. When subset gravity solutions (for example a complete fifth degree and order field) were sought from the Keplerian rate data generated from the seventh degree and order field, the numerical values obtained were very different from their nominal values. Basically the higher degree harmonics which had been omitted from the solution set were aliased into the lower ones due to the existing high correlations. Had a complete data set (data covering all latitudes and longitudes) been used, then orthogonality would have been induced in the $[G^TAG]^{-1}$ matrix and the subset values recovered would have been the nominal ones.

The discussion of the mascons and the lack of orthogonality associated with the Doppler data set is introduced as background for the rational process used in chosing a harmonic coefficient solution set. The basic strategy assumed in this analysis is to obtain the largest coefficient set possible while incurring a minumum of high correlations in the $[G^TAG]^{-1}$ matrix. It is a foregone conclusion that, with the data available at this time, it is not possible to detemine a lunar gravity field which truly represents all the localized fine structure near-surface mass inhomogeneities. The only attainable goal of this data analysis then is to derive a global lunar gravity model.

5. A Lunar Gravity Field

Solutions varying from degree and order three to degree and order seven were attempted from the one hundred ninety-nine sets of Kepler element rates. All solutions obtained above degree and order four contained very large numbers of high correlations in the solution $[G^TAG]^{-1}$ matrices. When these solutions were applied to tracking data from the Apollo orbits, both the fit and prediction characteristics obtained were very poor. As a result of this situation, the lunar harmonic coefficient set determined in this study is of degree and order four.

Analysis of the numerical characteristics of the full fourth degree and order solution revealed two important points. First, the C_{20} and C_{40} zonal coefficients were still highly correlated ($\varrho = 0.86$). Second, the solution contained very little direct information in determining the C_{22} harmonic. In performing the least-squares gravity estimation, the entry in the $G^TA\,\dot{\mathbf{k}}$ vector associated with C_{22} was essentially zero. (Other components were of significantly larger amplitudes.) Hence the estimate of C_{22} was dominated by correlations present in the $[G^TAG]^{-1}$ matrix. In order to circumvent these numerical problems, both the C_{20} and C_{22} terms were fixed in the gravity determination to values obtained by Koziel in studying the physical librations of the Moon. [14]

TABLE V

Gravitational field determined from Lunar Orbiters 1, 2, 3, and 5

l	m	$C_{lm} \times 10^4$	$S_{lm} \times 10^4$
2	0	−2.0560[a]	–
	1	0.0537	0.0617
	2	0.2258[a]	−0.0017
3	0	0.2216	–
	1	0.3575	0.0820
	2	0.0210	0.0340
	3	0.0301	0.0055
4	0	0.0543	–
	1	−0.0677	0.1195
	2	0.0443	0.0106
	3	0.0136	0.0066
	4	0.0027	0.0043

[a] Fixed in solution.

TABLE VI

Gravity solution correlation matrix

	C_{30}	C_{31}	C_{32}	C_{33}	C_{40}	C_{41}	C_{42}	C_{43}	C_{44}	S_{21}	S_{22}	S_{31}	S_{32}	S_{33}	S_{41}	S_{42}	S_{43}	S_{44}
C_{21}	−0.02	0.06	−0.11	0.11	0.25	0.59	−0.69	0.41	0.14	0.18	0.15	0.03	0.43	−0.08	0.3	0.21	0.05	0.25
C_{30}		−0.09	0.08	0.01	−0.39	0.17	0.08	0.01	0.03	−0.04	0.05	−0.05	0.19	−0.01	−0.05	0.06	0.01	0.07
C_{31}			−0.03	0.04	−0.34	0.18	0.1	0.05	0.05	0.33	−0.08	0.06	0.17	−0.05	0.56	0.01	0.29	0.00
C_{32}				0.06	0.01	−0.13	0.22	0.01	0.09	−0.18	0.33	−0.01	−0.15	−0.04	−0.2	0.81	0.23	0.13
C_{33}					0.03	0.07	−0.01	−0.01	0.28	0.04	−0.18	0.001	−0.02	−0.06	0.08	0.02	0.39	0.43
C_{40}						0.06	−0.11	0.21	−0.08	−0.12	0.07	0.01	−0.35	−0.02	−0.03	−0.24	−0.15	0.02
C_{41}							−0.53	0.43	−0.13	0.38	0.04	−0.64	0.4	−0.06	0.34	−0.11	0.17	0.15
C_{42}								−0.07	0.3	−0.15	−0.18	0.11	−0.66	0.12	−0.20	0.19	0.07	−0.11
C_{43}									−0.26	0.21	0.01	−0.16	−0.15	−0.34	0.36	−0.22	−0.01	0.04
C_{44}										−0.15	−0.13	0.02	−0.16	−0.4	−0.22	0.21	0.21	0.09
S_{21}											−0.23	0.13	0.18	0.09	0.84	−0.25	0.4	0.05
S_{22}												0.04	0.09	0.16	−0.18	−0.14	−0.12	0.33
S_{31}													−0.06	0.06	0.03	−0.02	−0.08	0.02
S_{32}														−0.06	0.06	0.08	0.1	0.04
S_{33}															0.07	0.04	0.05	0.11
S_{41}																−0.32	0.26	0.03
S_{42}																	0.24	0.21
S_{43}																		−0.06

The fourth degree and order field determined using this selenodesy method is given in Table V. The correlation matrix associated with this solution is given in Table VI. The A matrices used are not the covariance matrices of the element rates; hence, the terms on the diagonal of the $[G^T A G]^{-1}$ matrix cannot be regarded as the variances of the gravity coefficients.

The residuals associated with each of the five orbital element rates and this fourth order field are shown in Figures 6–8. These residuals have the statistical properties given in Table VII. As can be seen from the Kepler element rate residual plots, the errors are systematic in each case.

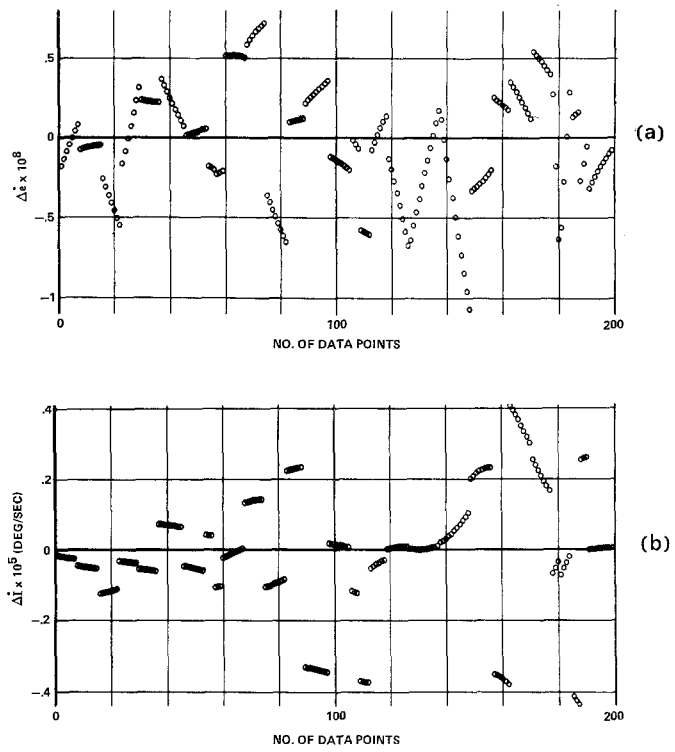

Fig. 6. (a) $\Delta\dot{e}$ and (b) $\Delta\dot{I}$ vs. number of data points.

TABLE VII

Kepler element rate residual statistics

Kepler element rate	Residual mean	Residual std. deviation
$\dot{e}$	-0.272×10^{-9}	0.345×10^{-8}
$\dot{I}$	-0.836×10^{-7} deg s^{-1}	0.170×10^{-5} deg s^{-1}
$\dot{\Omega}$	0.127×10^{-5} deg s^{-1}	0.265×10^{-5} deg s^{-1}
$\dot{\omega}$	-0.965×10^{-6} deg s^{-1}	0.374×10^{-5} deg s^{-1}
$\dot{M}$	0.915×10^{-7} deg s^{-1}	0.327×10^{-6} deg s^{-1}

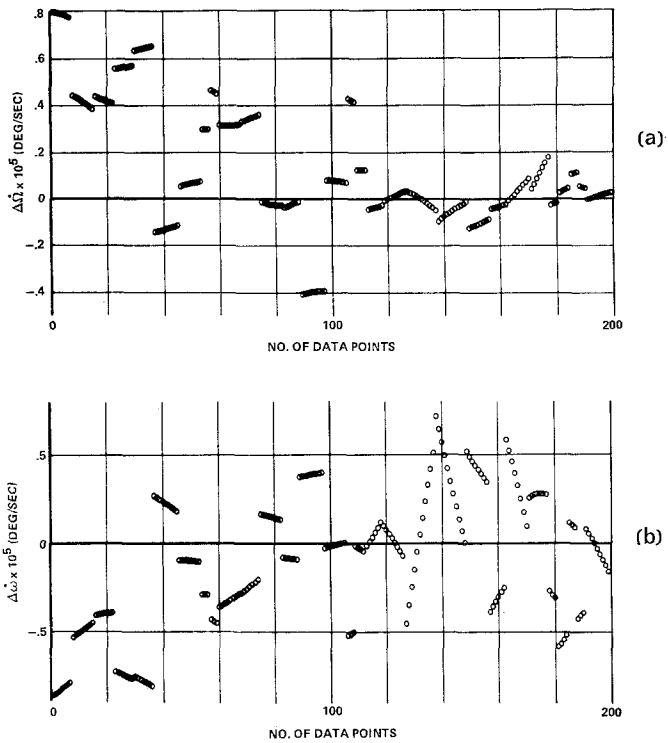

Fig. 7. (a) $\Delta\dot{\Omega}$ and (b) $\Delta\dot{\omega}$ vs. number of data points.

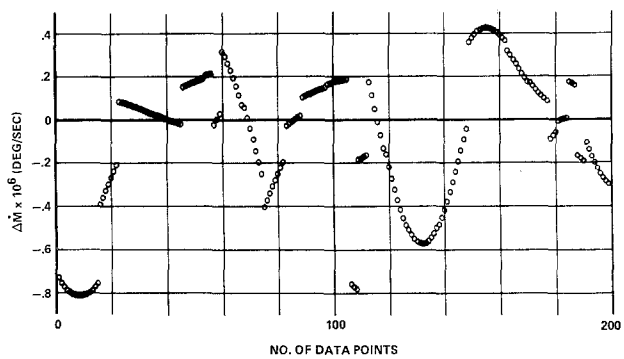

Fig. 8. $\Delta\dot{M}$ vs. number of data points.

Equipotential surfaces have been calculated for this lunar gravity field and are shown in Figures 9 and 10. These surfaces are computed by finding the radial deviations from a spherical potential (generated with the field point at the mean lunar radius). The variations are quantized in thousand foot increments. The basic equipotential surfaces of this gravity field are those of a triaxial ellipsoid. The solid line on the surfaces indicates the equipotential line for the reference potential (zero deviation

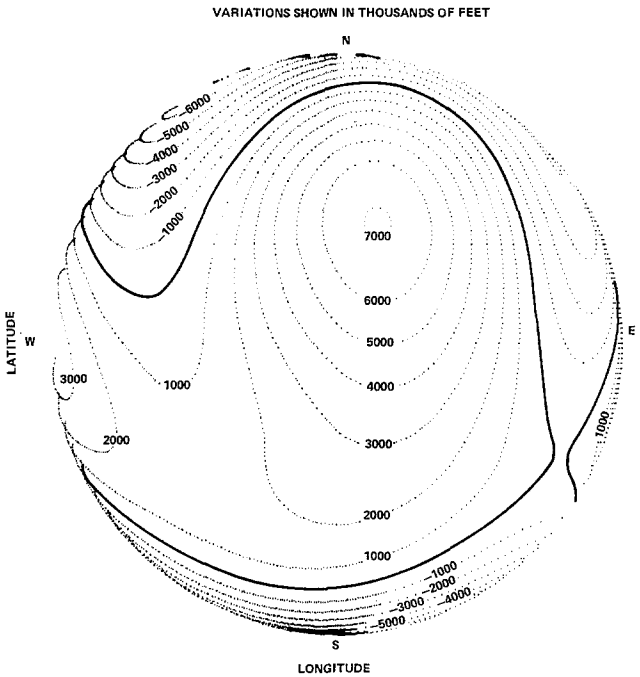

Fig. 9. Lunar near side equipotential surfaces.

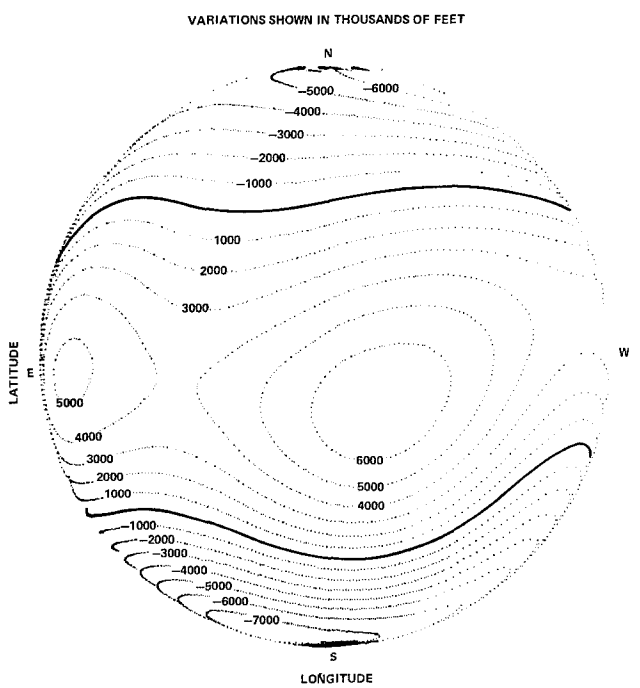

Fig. 10. Lunar far side equipotential surfaces.

from spherical potential). These surfaces show three large areas of potential excess. The first and largest of these is centered about latitude $\phi = 25°\,\mathrm{N}$ and longitude $\lambda = 10°\,\mathrm{E}$. This region very closely corresponds to the Mare Serenitatis region of the Moon. The two other areas of potential excess are located at latitude $\phi = 5°\,\mathrm{S}$, longitude $\lambda = 117°\,\mathrm{E}$ and latitude $\phi = 10°\,\mathrm{S}$, longitude $\lambda = 170°\,\mathrm{W}$, respectively. Neither of these two areas corresponds to an identified lunar maria region.

The second-degree harmonics in the potential are directly related to the moments and products of inertia of the Moon. The relations between the gravity coefficients and the moments and products of inertia are [15]

$$\begin{aligned} C_{20} &= \frac{1}{m_{\leftmoon} R_e^2}\left[\frac{A+B}{2} - C\right], \quad C_{22} = \frac{1}{4 m_{\leftmoon} R_e^2}(B - A), \\ C_{21} &= \frac{E}{m_{\leftmoon} R_e^2}, \quad S_{21} = \frac{D}{m_{\leftmoon} R_e^2}, \quad S_{22} = \frac{F}{m_{\leftmoon} R_e^2}, \end{aligned} \tag{11}$$

where $m_{\leftmoon}$ is the lunar mass, A, B, C are the three principal moments of inertia ($A = I_{xx}$, $B = I_{yy}$, $C = I_{zz}$) and D, E, F are the products of inertia ($D = I_{yz}$, $E = I_{xz}$, $F = I_{xy}$). Since Equation (11) contains five equations in six unknowns (A, B, C, D, E, F) one additional relationship is needed. From studies of the lunar physical librations the quantity

$$\beta = \frac{C - A}{B} \tag{12}$$

has been determined. The numerical value used is that computed by Koziel [14] from heliometer observations ($\beta = 6.294 \times 10^{-4}$). Hence given the five second-degree harmonics and β, the following set of principal moments and products of inertia is found:

$$\begin{aligned} A &= 0.398\,320\,8 \; m_{\leftmoon} R_e^2, & D &= 0.617 \times 10^{-5} \, m_{\leftmoon} R_e^2, \\ B &= 0.398\,411\,18 \; m_{\leftmoon} R_e^2, & E &= 0.537 \times 10^{-5} \, m_{\leftmoon} R_e^2, \\ C &= 0.398\,571\,95 \; m_{\leftmoon} R_e^2, & F &= -0.17 \times 10^{-6} \, m_{\leftmoon} R_e^2. \end{aligned} \tag{13}$$

The imprecision in the harmonics and the simplifications in the theory relating β to the inertias make the quality of these numbers somewhat poor.

6. Extrapolations

In order to measure the orbit determination and prediction qualities of the field obtained, it was applied to Doppler data not used in its generation. Specifically, the data used was acquired during the orbits of the Apollo 11, 12, 14, and 15 missions. The orbit determinations were performed using a standard least-squares processor which obtains a best estimate of a rectangular state vector at some epoch. This best estimate of the state is then used to predict the Doppler outside the span of data used for convergence.

Orbit determination solutions were obtained by fitting one front side pass of Doppler data from several tracking stations. This particular data length was chosen since it puts maximum stress on the orbital prediction capability of the model. Once a converged solution is obtained, the Doppler data are predicted for the next three orbital periods to test the extrapolation capabilities of the model.

The data used from Apollo 11 and 12 are from near-circular orbits with radius vectors of about 60 nautical miles (n.m.) above the lunar surface. The data from Apollo 14 and 15 are from slightly elliptical orbits ($e=0.0258$) with an apolune of 60 n.m. above the surface and a perilune of 8 n.m. above the surface. The data from the Apollo missions, since they are collected from orbits very near the lunar surface, reveal many gravitational perturbations not present in the Lunar Orbiter data.

Convergent solutions were obtained using the fourth degree and order gravity field. Doppler residuals for both the one pass fit and the three passes of prediction for each of these Apollo orbits are shown in Figure 11. The Doppler residuals in

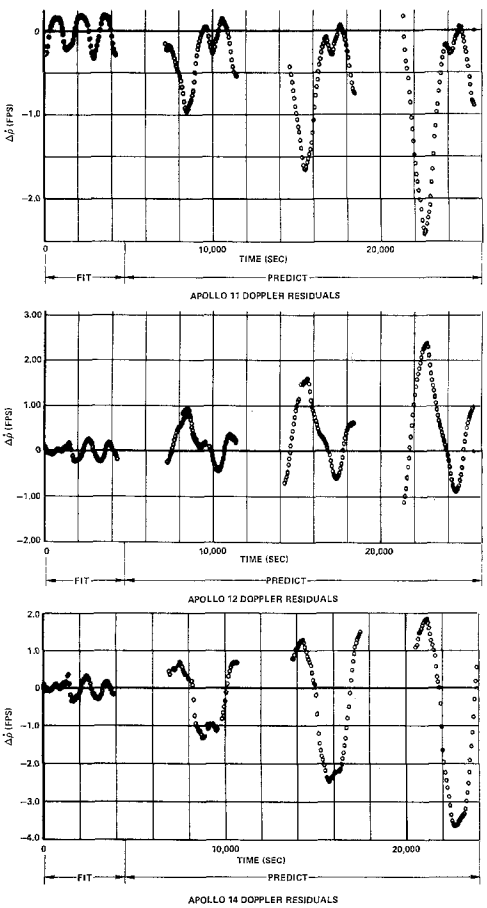

Fig. 11. Fourth-degree and order lunar gravity field.

each of these convergences are systematic and an order of magnitude above the noise level of the data. The three orbital period prediction is characterized by secular growth (period errors) in the residuals for each case. Both the systematic nature of the regressed Doppler and the growth in the Doppler residuals during the prediction reflect the incomplete nature of this fourth order field.

In order to obtain a relative perspective on the quality of orbit determination and prediction attainable, convergences were also performed on these data using two other gravity models. The first model, the L1 field, is used by the Manned Spacecraft Center for Apollo mission planning. The second model, developed by Liu and Laing [16], is a fifteenth degree zonal and eighth order tesseral model (84 terms) This model represents the latest research effort using the indirect analysis method [17].

Orbit determinations were again performed by fitting one pass of data and predicting the Doppler for the next three periods. The residuals associated with each of the fit and predictions for these two gravity models are shown in Figures 12 and 13.

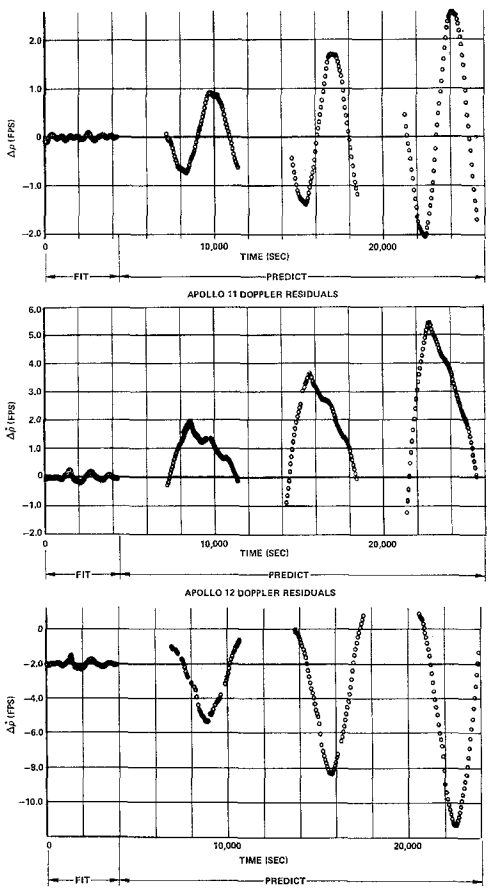

Fig. 12. L1 lunar gravity field.

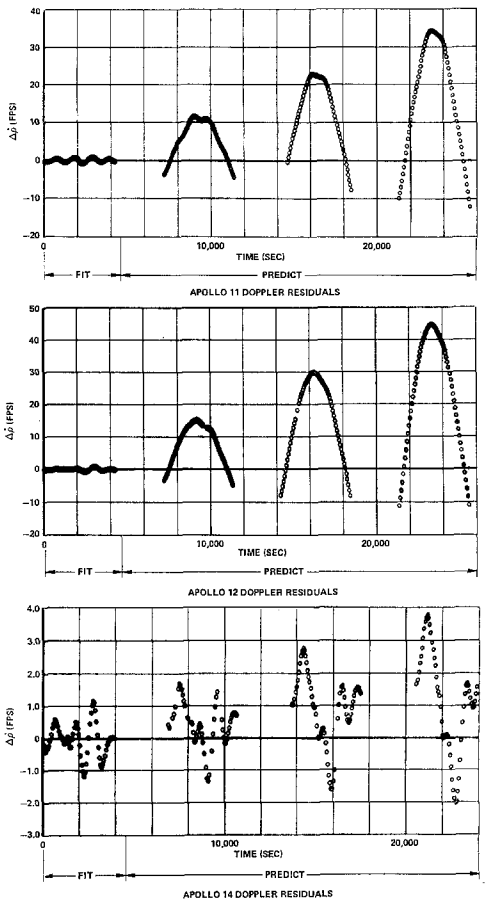

Fig. 13. Fifteenth-degree eighth-order lunar gravity field.

The Doppler residuals of the fit and prediction, for each field, have systematic errors. Both of these models, especially the fifteenth degree field, are characterized by secular growth in the Doppler residuals in the prediction. Table VIII lists the statistical properties of the one pass Doppler residuals for all three models. For these orbits, the L1 field achieves slightly better convergence statistics than the fourth order field. However, the fourth order field predicts the Doppler with an error rate of about 50% less than L1.

One pass fits and three pass predictions were also obtained using data from the Apollo 15 mission. The free-flight quality of these data is somewhat in doubt since the spacecraft was performing some minor propulsive thrusting. The Doppler residuals associated with the convergences of both the L1 and the fourth order field were larger than those of any other Apollo orbits. The complete statistical properties for the one pass Apollo 15 residuals for all three models are listed in Table VIII. The Doppler residuals of the three period prediction exhibited an inordinately large

TABLE VIII
Apollo convergence statistics

Orbit	Model	Residual mean (FPS)	Std. deviation (FPS)
Apollo 11	4×4[a]	−0.011	0.166
	L1	−0.0015	0.039
	15×8[b]	−0.023	0.463
Apollo 12	4×4	−0.0029	0.136
	L1	−0.0042	0.104
	15×8	−0.022	0.353
Apollo 14	4×4	−0.0016	0.187
	L1	−0.0055	0.159
	15×8	−0.0304	0.526
Apollo 15	4×4	0.0054	0.385
	L1	−0.0055	0.252
	15×8	−0.0042	0.400

[a] Fourth-degree and order model
[b] Fifteenth-degree and eighth-order model

secular growth for each model. The growth rate in the residuals for each of these models is as follows:

Model	Doppler residual Growth/period (FPS)
L1	30
4×4	46
15×8	100

Since the Apollo 15 trajectory passed over some of the largest mascon basins on the Moon, this large growth in the Doppler residuals is probably due to the effects of unmodeled mascons. The quantitative effects of having some minor thrusting in the orbit are difficult to evaluate, hence it is nearly impossible to integrate this factor into the Doppler growth rate experienced.

7. Summary and Conclusions

An empirical method for determining the spherical harmonic coefficients of the lunar gravity field has been presented. The method has been applied to Doppler data from the Lunar Orbiter 1, 2, 3, and 5 satellites. A gravity field of degree and order four is derived from these data. Equipotential surfaces from this gravity field show the lunar mass distribution to be that of a triaxial ellipsoid with three large areas of mass concentration. The largest and by far the most dominant of these areas is centered very near the Mare Serenitatis region and covers a large portion of the near side of the Moon. The other two regions of mass concentration are located on the far side of the Moon but do not correspond to any specific mare region.

This gravity field has been investigated using data from several of the Apollo missions. Orbit determination solutions from these data show that, in all cases except that of Apollo 15, this fourth order field results in improved orbit predictions as compared to those using other gravity fields. All solutions indicate the lunar field models are still incomplete.

References

[1] Caputo, M.: 1967, *The Gravity of the Earth from Classical and Modern Methods*, Academic Press, New York.
[2] Kaula, W. M.: 1966, *Theory of Satellite Geodesy*, Blaisdell Publishing Co., Waltham, Mass.
[3] Lorell, J. and Liu, A.: 1971, 'Method of Averages Expansion for Artificial Satellite Application', Jet Propulsion Laboratory Report 32-1513.
[4] Kozai, Y.: 1961, 'Effects of Solar Radiation Pressure on the Motion of an Artificial Satellite', Smithsonian Institution, Special Report No. 56.
[5] Ferrari, A. J.: 1971, 'Lunar Gravity Derived from Long-Period Satellite Motion – A Proposed Method', Bellcomm, Inc., TM71-2014-6.
[6] Izsak, I. G.: 1961, 'Differential Orbit Improvement with the Use of Rotated Residuals', Smithsonian Institution, Special Report No. 73.
[7] Wollenhaupt, W. R.: 1970, 'Apollo Orbit Determination and Navigation', Presented at AIAA 8th Aerospace Sciences Meeting, New York, N.Y.
[8] Kozai, Y.: 1959, *Astron. J.* **64**, 378.
[9] Kozai, Y.: 1962, *Astron. J.* **67**, 446.
[10] Durbin, J.: 1960, *Revue Inst. Int. De Stat.*, p. 233.
[11] Battin, R. H.: 1964, *Astronautical Guidance*, McGraw-Hill Book Co., New York.
[12] Peabody, P. R., Scott, J. F., and Orozco, E. G.: 1964, 'Users Description of JPL Emphemeris Tapes', Jet Propulsion Laboratory Report No. 32-580.
[13] Muller, P. M. and Sjogren, W. L.: *Science* **161**, 3842.
[14] Koziel, K.: 1967, *Icarus* **7**, 1.
[15] Michael, W. M. *et al.*: 1970, in Bruno Morando (ed.), *Dynamics of Lunar Satellites 1969*, Springer-Verlag, Berlin, pp. 42–56.
[16] Liu, A. S. and Laing, P. A.: 1971, 'Lunar Gravity Field as Determined by Orbiters', Presented at 14th Planetary Meeting of COSPAR, Seattle, Washington.
[17] Lorell, J.: 1970, *The Moon* **1**, 190.